Non-linear frequency response analysis for assessment of the ageing history of lithium ion batteries: A combined simulation and experimental approach

Ottakath Cholakkal, S. R., Shepherd, S., Kellner, Q. & Curnick, O.

Published PDF deposited in Coventry University's Repository

Original citation:
Ottakath Cholakkal, SR, Shepherd, S, Kellner, Q & Curnick, O 2024, 'Non-linear frequency response analysis for assessment of the ageing history of lithium ion batteries: A combined simulation and experimental approach', Journal of Energy Storage, vol. 86, no. Part B, 111265.
https://dx.doi.org/10.1016/j.est.2024.111265

DOI 10.1016/j.est.2024.111265
ISSN 2352-152X
ESSN 2352-1538

Publisher: Elsevier

This is an open access article under the CC BY license
(http://creativecommons.org/licenses/by/4.0/)

Journal of Energy Storage 86 (2024) 111265

Contents lists available at ScienceDirect

Journal of Energy Storage

journal homepage: www.elsevier.com/locate/est

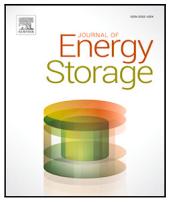

Research papers

Non-linear frequency response analysis for assessment of the ageing history of lithium ion batteries: A combined simulation and experimental approach

Safeer Rahman O.C. [a,*], Simon Shepherd [a], Quirin Kellner [b], Oliver Curnick [a]

[a] Centre for Advanced Low Carbon Propulsion Systems (C-ALPS), Coventry University, Coventry, CV12TL, England, United Kingdom
[b] FEV UK LTD, Coventry, CV12TL, England, United Kingdom

ARTICLE INFO

Keywords:
Lithium battery
Ageing modes
Nonlinear frequency response analysis
Change in harmonics

ABSTRACT

In this work, we present a novel approach for identifying the ageing history of lithium-ion batteries based on experimental nonlinear frequency response analysis (NFRA) measurements. A regression model, trained on simulated NFRA data, is shown to be capable of quantifying degradation modes such as solid electrolyte interphase (SEI) growth, lithium plating, and loss of active material (LAM) with no a-priori knowledge of the cell's historical duty. Our analysis, combining experimental and simulation approaches, demonstrates NFRA's potential as a powerful tool for ageing diagnosis by capturing various degradation modes. Changes in NFRA response through life exhibit strong correlations with ageing paths, particularly in the frequency range of 0.2 to 10 Hz. Observations highlight a strong influence of the state of charge on the resultant NFRA response, emphasizing that measurements at a single open circuit voltage (OCV) and harmonics values from a single frequency are insufficient for comprehensive characterization. This analysis underscores the need for correlating NFRA at multiple OCVs and frequencies for detailed ageing assessment. Evaluation on commercially relevant cells enhanced the models' reliability for industrial applications. This quantitative, data-driven approach using NFRA holds potential to enhance battery management strategies, extend lifespan and improve confidence in second-life applications of batteries. Future work should focus on improving regression analysis robustness, reducing dimensionality, and broadening testing conditions.

1. Introduction

Understanding the impact of various ageing mechanisms inherent in lithium-ion batteries on the overall capacity loss during their life cycle is crucial for optimizing their performance, longevity, and safety. This understanding becomes particularly crucial in automotive applications where batteries are operated under diverse duties and environmental conditions and are subjected to significant stress during their operational lifespan. The comprehensive understanding of the ageing history of lithium-ion batteries also holds significant importance in the context of future second life applications, which involve utilizing batteries, previously aged in primary applications such as in the automotive industry, for other uses like energy storage for stationary applications. Assigning an accurate market value to a used battery asset requires the knowledge of its ageing history and, in turn, its likely remaining useful life. This underscores the critical need for developing improved diagnostic methods and accurate models for precise evaluation of different ageing losses to ensure sustained and reliable performance of lithium-ion batteries throughout their life.

The ageing of lithium-ion batteries in general is observed outwardly as the reduction in capacity and the increase in the battery impedance. However, internally at the microscale, battery degradation proceeds via a complex set of interacting processes, driven and influenced by various factors such as high charge–discharge rates, extreme temperatures and mechanical stresses. Several studies have conducted detailed analyses of various ageing processes, examining their potential impacts and underlying causes [1–4]. The degradation of lithium ion batteries results from complex interactions, but can be predominantly characterized in two major modes of degradation, reduction in recyclable-lithium ions (loss of lithium ion inventory—LLI) and reduction in the amount of active materials (loss of active material—LAM) [1] in both negative and positive electrode. Out of these two degradation modes, the widely reported major degradation paths are SEI formation, lithium plating leading to LLI and the LAM due to change in electrode material structure caused by mechanical stress. In this study the emphasis is on identifying the SEI layer growth, lithium plating and active material loss in negative electrode.

The SEI is a thin film that forms on the negative electrode's surface due to a chemical reaction between the liquid electrolyte and the electrode's conductive layer. Initially, this layer impedes further

* Corresponding author.
E-mail address: ottakathcs@coventry.ac.uk (Safeer Rahman O.C.).

https://doi.org/10.1016/j.est.2024.111265
Received 22 December 2023; Received in revised form 19 February 2024; Accepted 10 March 2024
Available online 16 March 2024
2352-152X/© 2024 The Authors. Published by Elsevier Ltd. This is an open access article under the CC BY license (http://creativecommons.org/licenses/by/4.0/).

electrolyte reactions, but as cells age, its thickness usually increases. Factors contributing to this growth include high current and temperatures. Elevated temperatures accelerate diffusion rates, consequently increasing the rate of SEI growth. Similarly, high currents induce particle cracking, fostering the formation of new SEI layers [2]. Lithium plating, a parasitic reaction occurring during charging, involves the formation of metallic lithium instead of the intended intercalation into the graphite anode structure. This phenomenon is more pronounced with high charging currents at low temperatures where intercalation rates are significantly reduced. Dendrites are formed from lithium plating, can breach the separator, potentially causing internal short circuits and thermal runaway. Charge discharge cycles can lead to stress and structural changes in the electrode materials. For graphite electrode lithiation leads to volume expansion and de-lithiation causes contraction, which lead to cracks in the electrodes. High charge discharge rates often enhance the cracking and this leads to the LAM and can cause both capacity reduction and power fade [1].

Even though many methodologies and models used for identification of battery state of health (SOH) have been reported [5], due to its complexity quantification of ageing path during life time operation less is explored. At present, the literature in this field is sparse and the exploration of reliable and practical diagnostic techniques for quantifying the contributions of various individual degradation modes to overall State of Health (SOH) losses is still in its early stages. Teliz et al. proposed a method to identify and measure the ageing mechanisms in lithium-ion batteries using electrochemical impedance spectroscopy (EIS). They fitted EIS spectra at a single state of charge(SOC) to a second order equivalent electrical circuit model, whose parameters were then used to predict the extent of individual degradation mechanisms (SEI, LLI, LAM) in the batteries aged through cycling at two C-rates [6]. However, for a more comprehensive understanding, it is essential to assess the EIS-based method's performance on batteries aged under varied temperatures to ensure its broader applicability. The study [7] investigates ageing mechanisms of lithium-ion batteries using half-cell and full-cell open-circuit voltage (OCV) characteristics and developed a model to identify ageing mechanisms based on changes in the full-cell OCV characteristics. However the experimental measurements used by this method require over 50 h and therefore not suitable for high-throughput battery grading or re-manufacturing.

Here, we introduce Non-linear Frequency Response Analysis (NFRA) as an alternative method for quantifying degradation modes in lithium-ion batteries. In recent years NFRA has emerged as a valuable tool for lithium-ion batteries, demonstrating its effectiveness in process identification [8], state-of-health (SOH) diagnosis [9,10], and lithium plating detection [11]. While Harting et al. and Wolff et al. have highlighted NFRA's applicability, further exploration under diverse ageing conditions and varying states of charge is needed. It is important to note that the exploration of NFRA's application in this context of lithium ion batteries is still in its early stages, with a limited body of work currently available.

2. Methodology

As there are limited practical diagnostic techniques capable of distinguishing different degradation modes, our approach uses a detailed pseudo two dimensional (P2D) model to simulate ageing alongside periodic, simulated NFRA measurements at well defined SOHs. Crucially, the P2D model is able to track the progression of individual ageing modes. The overall methodology of this study includes a comprehensive collection of data through both experimental and simulation approaches. The NFRA responses at diverse ageing conditions were simulated and then the harmonic features were extracted from these simulations. The harmonic features obtained at the aged conditions were compared to the initial cell simulation data and the delta values were used in regression analysis based on a random forest approach to correlate these data with the ageing modes. The outcome of this analysis facilitated the development of distinct models for the three primary degradation modes mentioned; SEI growth, Lithium plating, and LAM. Subsequently, to evaluate the impact of ageing conditions, the NFRA data gathered from cells cycled under various conditions were applied to these regression models. The entire process is illustrated in Fig. 1, and detailed explanations of each step are provided in the following sections.

2.1. Non linear frequency response analysis- NFRA

The NFRA measurement technique involves the application of relatively large sinusoidal currents across the battery cell, with amplitudes (I_{amp}) typically in the range 1 to 3C at frequencies ranging from 10 millihertz (mHz) to 1 kilohertz (kHz). This contrasts with EIS, which shares a similar frequency-based approach but typically utilizes smaller amplitude perturbations. The time-dependent changes in the sinusoidal output voltage are captured by applying a Fast Fourier Transformation (FFT). The FFT transforms signal from the time domain to the frequency domain, revealing not only the voltage response corresponding to the input fundamental frequency Y_F, but also the higher harmonic responses Y_n with n ≥ 1. The non-linear processes inherent in lithium-ion batteries are expected to generate higher harmonics. In general, it was observed that the harmonic magnitudes were significantly attenuated as the harmonic order increased [10]. In this study, we focus primarily on the first two higher harmonics, Y_2 and Y_3. However, we have also considered the total harmonic distortion (THD), Y_{thd} and the ratio of Y_2, Y_3 as a measure of the amount of distortion present in the response voltage. THD is calculated as the root mean square (RMS) value of the higher harmonics. Higher-order harmonics (n ≫ 3) were not considered as they were typically in the noise level of the instrument and could not be measured accurately [10,12].

2.2. Experimental

The lithium ion cell selected for this investigation was the commercially available LG M50 21700 NMC811 cylindrical cell, with a nominal capacity of 4.85 Ah. To assess varied cyclic ageing characteristics, the cells were subjected to temperature controlled cycling at five distinct temperatures (50 °C, 45 °C, 25 °C, 10 °C, and −5 °C) and two different C-rates. The cycling involved charging and discharging at 1C and 0.5C rates. This charge–discharge cycling is detailed in Table 1. Performance tests were performed at regular intervals during cycling, which include capacity testing and NFRA tests at three different states of charge (SOCs) corresponding to the open circuit voltages (OCV), 3.3, 3.6 and 3.9 V with an amplitude of 2C(9.3 A). In accordance with earlier reported work [10] a minimum amplitude of 1.5 C is recommended for higher harmonics analysis of lithium ion cells. However, to ensure a comprehensive exploration of the system dynamics and to guarantee a meaningful non linear response, we have opted to perform our experiments with a 2C amplitude. The cells were equilibrated to an ambient temperature of 25 °C before the capacity and NFRA tests. Cyclic ageing was performed using the Neware cell cycler (BTS400). The Ivium-n-stat(5 V 10 A module) was used for the NFRA measurements. The details of experimental process are illustrated in the flowchart given in Fig. 2, which includes the sequential test procedures and ageing protocol as outlined in Table 1. The performance test referred in Fig. 2 includes the capacity and NFRA test.

In NFRA measurements, a logarithmic sweep comprising 50 frequency points, ranging from 1 kHz to 0.01 Hz was conducted for harmonic analysis. The amplitude throughout the sweep was maintained at a constant value of 2C. To eliminate the influence of the fundamental frequency response on the higher harmonics and in the THD calculation, the values where normalized by the fundamental amplitude and the percentage value is calculated as given in Eqs. (1) and (2). In this study, frequency values in the sweep are denoted as f_1

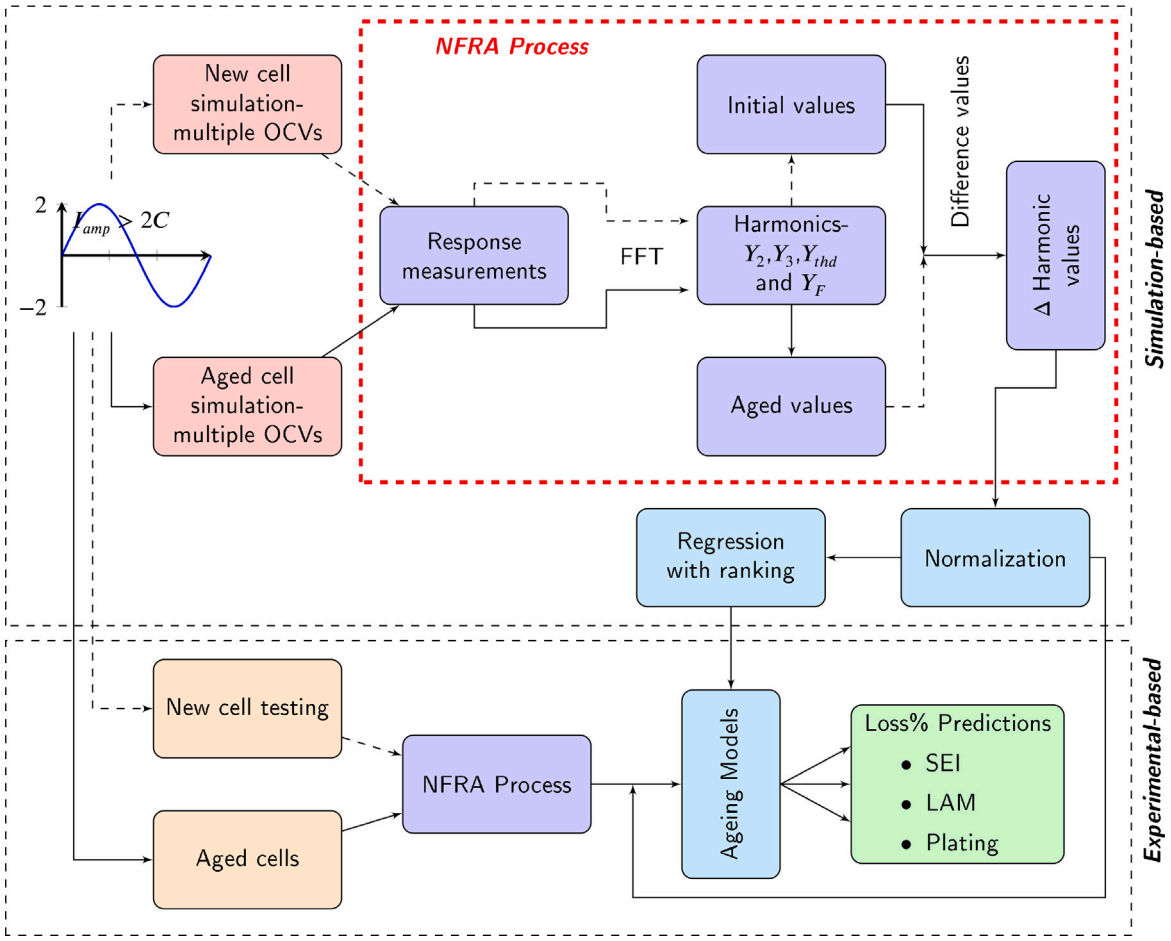

Fig. 1. The process flow of regression model development and experimental testing.

Table 1
Cell cycling protocol.

Step	Time	End condition
Charge CC-CV (1C/0.5C)	–	4.2 V, 200 mA
Rest	0.5 h	–
Discharge CC (1C/0.5C)	–	2.5 V
Rest	1 h	–

for 1 kHz and f_{50} for 0.01 Hz, serving as references for our subsequent discussions and analyses.

$$Y_n\% = \frac{Y_n}{Y_F} * 100 \tag{1}$$

$$Y_{thd}\% = \sqrt{\frac{(Y_2\%)^2 + (Y_3\%)^2}{2}} \tag{2}$$

2.3. Simulation methods

2.3.1. PyBaMM

In this study, the Python-based multi-physics battery modelling software package PyBaMM (Python Battery Mathematical Modelling) is utilized for P2D modelling to generate simulated data [13]. The employment of modelling techniques present a cost-effective and time-efficient approach for examining diverse phenomena compared to experimental methods. Notably, given the intricate nature of ageing processes and their potential simultaneous occurrences, modelling serves as a valuable tool to isolate and assess individual ageing processes effectively. PyBaMM's modular architecture makes it easy to add new features and functionality without having to make major changes to the existing code. This makes it easier to employ new models and numerical methods. The Doyler Fuller Newman (DFN) model package available in PyBaMM is used to simulate the beginning of life performance of the cells. As explained in Section 1, to consider the main ageing modes, the following sub models were added individually and in combination: SEI growth: SEI-solvent-diffusion limited Lithium plating: partial reversible and irreversible Loss of active material: stress-driven Detailed simulation parameters and conditions are elucidated in Section 3. However, the model formulations and considerations pertaining to the SEI, lithium plating, and LAM submodels will not be elaborated here. Interested readers are referred to the comprehensive works of O'Kane et al. for an in-depth understanding [2,14]. PyBaMM was used to simulate DC charge/discharge characteristics in addition to AC impedance measurements. For AC simulations, a time-domain sinusoidal current was defined and iterated over the same frequencies used in experimental measurements, further details are explained in Section 2.3.

2.3.2. Model parameters

The simulations were conducted utilizing the default Okane2022 parameter sets tailored for LG M50 cylindrical cells, which were developed based on the work of Chen et al. [15]. These parameters still required some adjustment to achieve a satisfactory alignment with experimental data. The identification of sensitive parameters and their refinements were guided by the work of Budhi et al. [16]. The changed parameter set is detailed in Table 2. Fig. 3(a) displays both experimental and simulated discharge curves with tuned parameters for 0.2C and

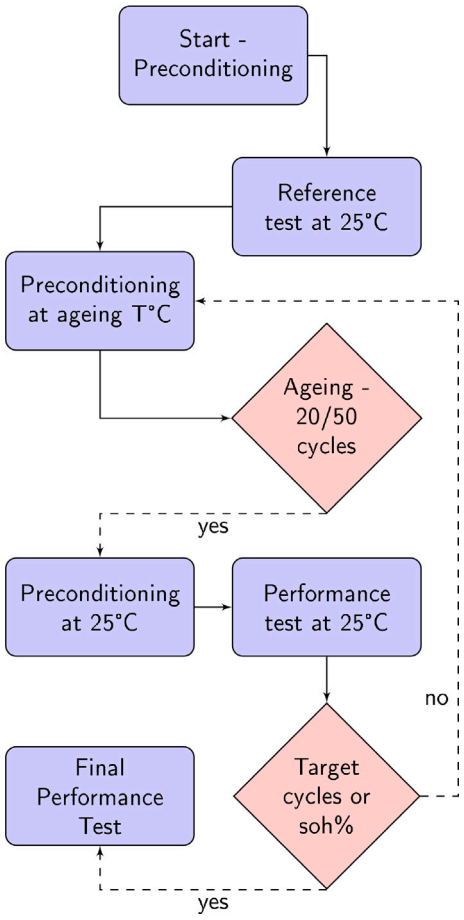

Fig. 2. Experiment process flow (Performance test includes capacity check and NFRA test).

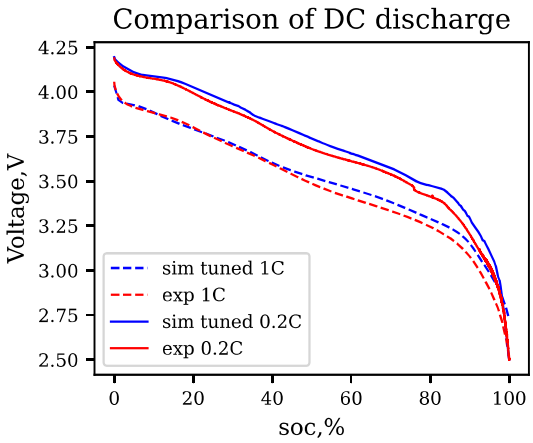

(a) Simulation vs. experiment 0.2C and 1C discharge profile

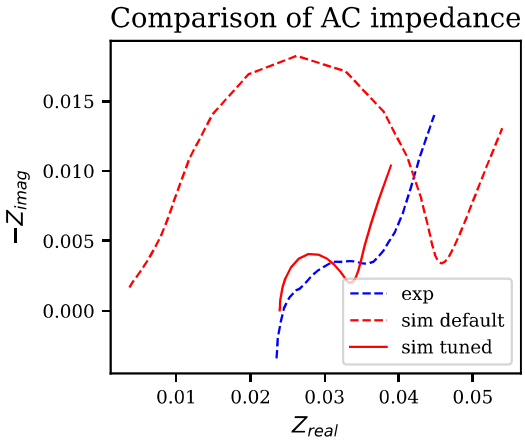

(b) Simulation vs. experiment EIS Curve

Fig. 3. Comparison of experimental and simulation results for new cells.

1C DC discharges respectively and a very good fit was obtained. The simulated DC curves showed minimal change with default parameters and tuned parameters. Meanwhile in Fig. 3(b) the Nyquist EIS plot comparison is presented, showcasing the model's capability to simulate AC impedance responses. The simulated EIS plot using tuned parameters demonstrates a robust qualitative alignment with experimental data, effectively capturing key features such as the semicircular region indicative of charge transfer and the diffusion tail observed in the lower frequency range. However, it is essential to acknowledge certain quantitative disparities between the experimental and simulated values. For instance, the absence of initial inductive part observed in the experimental data and warrants further investigation and refinement. Despite this disparity, the overall agreement between the simulated and experimental results are promising, providing a solid foundation for ongoing research and paved the way for further exploration of diverse ageing simulations by invoking different ageing sub models. For better AC simulation, the **surface form: differential** sub model was required to be used. This specific sub model, implemented within the PyBaMM framework, plays a pivotal role in capturing and representing the dynamic behaviour of the system at the surface level [13].

Additionally, to enhance solver performance and achieve more effective outcomes, the default value for spatial discretization in PyBaMM was finely tuned, specifically adjusted to 30. The simulations were conducted under isothermal conditions, prompted by the unavailability of precise thermal parameters. This simplification is justified by the findings in [11], which demonstrated the negligible impact of internal cell heating on NFRA spectra. Furthermore, our experimental observations align with this assertion, revealing minimal temperature changes during NFRA measurements.

2.4. Regression analysis

In an earlier study by Harting et al. [9], a data-driven model was developed to correlate NFRA results with the battery health. Their findings indicated an increase in Y_{thd} values observed at a singular state of charge (SOC-50%) with ageing. They developed a model correlating y-intercept data of Y_{thd} frequency plot to the SOH. However, previous work in our group [12] and current study reveals that the NFRA outcomes vary depending both on the battery's SOC and the frequency of testing. Specifically, the observations indicated a decrease in Y_{thd} at lower SOCs with ageing. Also, it is shown that the similar SOH cells aged at different temperature, had shown difference the Y_{thd} response with cold temperature aged cells having higher THD value. This possibly suggests that the existence of diverse ageing mechanisms can impact harmonics at different SOCs, creating challenges for characterizing ageing using only single NFRA response parameter and values obtained at a single OCV. Here in the study, we observed that rather than directly utilizing the harmonic values (Y_2, Y_3) obtained at various frequencies, the change of these values during ageing from the pristine cell (ΔY_n) calculated as given in Eq. (3) offered a more insightful perspective. Further details of these observations and analysis are explained in the result and discussion, Section 3.

$$\Delta Y_n\% = Y_{n^{th}cycle}\% - Y_{initial}\% \tag{3}$$

In order to quantify degradation modes based on NFRA results data analysis techniques were employed. Random Forest Regression Analysis

Table 2
Tuned parameters.

Parameter	Default value	Tuned value
Positive and negative particle radius [m]	5.22e−6, 5.86e−6	1.22e−6, 1.86e−6
Positive and negative electrode solid diffusion coefficient	4e−15, 3.3e−14	1e−15, 5e−15
Electrolyte conductivity and diffusivity coefficient	1.7e3, 1.7e4	0.26e3, 8.5e4
Positive and negative electrode double-layer capacity [F m^{-2}]	0.2, 0.2	4, 10
Positive and negative current collector conductivity [S m^{-1}]	3.69e7, 5.84e7	3.41e5, 5.81e5

Table 3
Ageing parameter set.

Ageing submodel	Parameter in PyBaMM	Range of values used
SEI Growth	Outer SEI solvent diffusivity	1e−23 to 1e−17
Plating - Partially reversible	Lithium plating kinetic rate constant	1e−14 to 5e−9
Irreversible	Dead lithium decay constant	1e−6 to 1e−3
LAM- Negative electrode	Positive electrode LAM constant proportional term	1e−4 to 8e−1

was used to study and develop a correlation model between NFRA responses and various ageing modes. A well-trained Random Forest model can make predictions efficiently, even in real-time or near real-time scenarios, making it suitable for BMS applications and at diagnostic centres.

3. Results and discussion

3.1. NFRA ageing characteristic from experimental results

As discussed in Section 2.2, the cells were cycled at distinct ambient temperatures and charging rates aimed at inducing capacity fade through diverse mechanisms. For each of the conditions a total of 3 cells were cycled. A clear trend of decreasing $Y_{thd\%}$ was observed with decreasing SOH at the lower OCV (3.3 V) for all ageing experiments. Fig. 4(a) displays this trend for a representative results of $Y_{thd}\%$ for cyclic ageing at 25 °C 1 C charge–discharge. The NFRA spectra for different aged cells exhibited significant variations in the frequency range of 0.01 to 10 Hz. As shown in Fig. 4(b), the harmonic response of the cell demonstrates considerable variation with Open Circuit Voltage (OCV), notably with higher $Y_2\%$ values observed at lower OCV in agreement with [12]. A parallel trend was observed for the higher harmonic $Y_3\%$, however with a substantially lower magnitude compared to $Y_2\%$. While the harmonics values showed differences, the nature of spectra remained similar The NFRA dependency on the ageing path was more evident from the distinctive nature of $\Delta Y_n\%$ curves, which represent the changes in NFRA values from their initial states. $\Delta Y_{thd}\%$ obtained for a similar extent of degradation (soh ~93%) but subjected to different ageing temperatures (−5 °C and 45 °C) are shown in Fig. 4(c). Lower temperature ageing, indicative of potential plating, exhibited a negative slope in the characteristic frequency range. Conversely, higher temperature ageing, suggestive of predominant SEI growth, demonstrated an opposite trend. These findings underscore the correlation between NFRA results and ageing modes, revealing a high level of complexity in the ageing processes. To further extend our analysis, we recognized the necessity of exploring a more comprehensive parameter space and decided to use physics-based modelling, employing the PyBaMM P2D model. This modelling approach provided a detailed investigation into the battery's behaviour, facilitating a deeper exploration of the observed phenomena. The outcomes of this modelling effort, along with the model development process, are presented in Section 3.2. The key findings from the experimental results are that the change in NFRA responses for cells aged to similar soh via different modes were markedly different, and NFRA responses were highly dependant on SOC as reported by [12].

3.2. NFRA ageing characteristic from simulation results

The simulations conducted in this study were intended to generate a training dataset for the subsequent regression modelling task, containing simulated NFRA spectra for cells having undergone simulated ageing under a broad range of conditions. The ageing sub models integrated in PyBaMM are formulated to capture the dependency of temperature and charge/discharge duty on ageing parameters. Hence temperature and C-rates were not considered as predictors for the regression analysis. To isolate the effects of individual degradation modes on NFRA responses, the main parameters governing their respective rates were varied, within the numerical range detailed in Table 3. In accordance to the previous works [14], the negative electrode often undergoes more pronounced degradation hence the emphasis of LAM ageing in the simulations is on negative electrode material loss.

Ihe NFRA simulations were performed at multiple OCVs at regular intervals of SOH values. A qualitative and quantitative similarity between the simulated spectra and experimentally obtained spectra was observed. However, minor deviations were encountered, which could be attributed to inherent complexities in the simulation models or potential experimental variabilities. Fig. 5 illustrates the simulated harmonic responses $Y_{thd}\%$, for a pristine cell at different OCVs, demonstrating the concordance between simulation and experimental outcomes. The absolute magnitudes of the $Y_{thd}\%$ responses are broadly similar (in the range 0%–6%) in simulated and experimental measurements, and characterized by a roll-off towards 100 Hz. The distinct peak observed around 7 Hz in the simulated NFRA response contrasts with its limited presence in the experimental data at 3.3 V. Notably, this characteristic peak only emerged at higher OCVs (>3.5 V) in the experimental measurements, as illustrated in Fig. 4(b). Whilst there is clearly not precise quantitative agreement between the experimental and simulated NFRA responses shown in Figs. 4 and 5, respectively, there are qualitatively similar trends. Both experimental and simulated NFRA spectra are characterized by local peaks in THD around 7 Hz, a general increase in THD towards lower frequencies and roll-off at higher frequencies. The general increase in THD at lower OCVs illustrated in Fig. 4(b) is consistent with previous experimental studies [12], and is replicated by the simulated data shown in Fig. 5, although the increased responses appears at OCVs < 3.1 V in simulations, versus < 3.3 V in experimental data. This general qualitative agreement is considered sufficient for the purposes of this exploratory study on the effects of ageing mechanisms on NFRA response.

To reduce any systematic error due to difference in quantitative agreement between experimental and simulated NFRA responses, we adopted a strategy of computing the difference between spectra of aged cells and their corresponding initial values. This approach is motivated by the expectation that distinct ageing modes will result in variations across different frequency regions, emphasizing the focus on observed

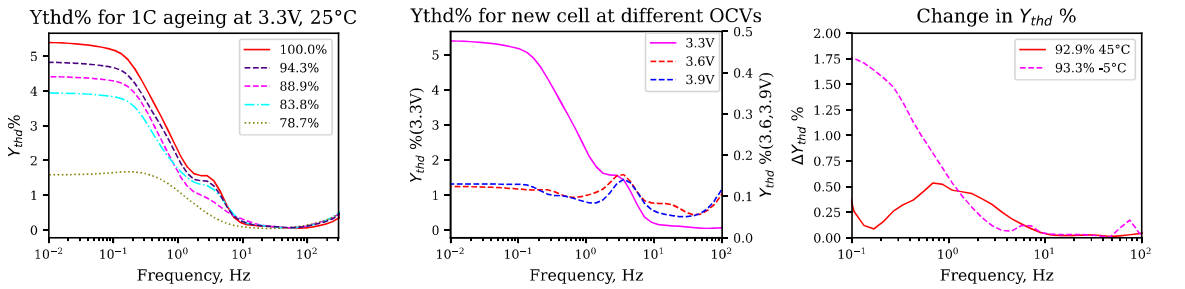

(a) Y_{thd}% trend with ageing. (b) Y_{thd}% trend with OCV (c) ΔY_{thd}% for different ageing conditions

Fig. 4. Comparative analysis of Y_{thd}% characteristics from experimental data.

variations rather than the specific values. PyBaMM ageing simulation cycles were executed in such a way that solution files and parameter sets obtained at the conclusion of each targeted SOH level were stored and subsequently utilized as inputs for NFRA simulations. Sinusoidal currents were generated using a current function class and five cycles for each chosen frequency were applied. Following this, from the output voltage obtained, the fifth cycle was then subjected to FFT analysis. In order to enhance the resolution of harmonic peaks, last cycle output voltage was extended to 500 cycles, each subdivided into 500 time steps, with a time step size of $\frac{1}{500\times\text{frequency}}$ per cycle before applying FFT. The '**fft**' package from Python's **Scipy** library was employed for this analysis. The DC component was eliminated by subtracting the mean value from the original voltage signal. Fig. 6 presents 3D characteristic spectra illustrating variation of the ΔY_{values}% response, with frequency, and OCV, for simulated individual ageing mechanisms plating, LAM and SEI growth. By inspection, it is apparent that the different ageing mechanisms result in markedly different NFRA responses within this parameter space. Observations indicate a generally larger change in Y_2% is compared to change in Y_3%, particularly the ΔY_2% (Fig. 6(f)) has a much larger value for LAM ageing. As a result, the ΔY_{thd}% exhibits a similar trend to ΔY_2%. It can be seen that LAM ageing induces an increase in Y_2% and Y_{thd}% within the mid OCV region (3.3 to 3.5 V), while plating manifests effects in the lower region (2.8 to 3.1 V) and at higher OCV (near to 4.1 V). In case of SEI growth, it shows a consistent influence throughout the SOC range, but with increased variability around 3.1 V region (Fig. 6(e)). Regarding ΔY_3%, SEI ageing appears to have consistent variation expect for the higher voltage region. For LAM ageing, ΔY_3% is dominant (Fig. 6(h)) in mid ocv region but it is much lesser compared to the change in Y_2%, how ever in case of plating it can seen that in Fig. 6(g) in the OCV region (3.3 to 3.5) there is a significant change in Y_3% comparable to change in Y_2% observed in Fig. 6(d). The variations in fundamental repose $\Delta Y_F(V)$, representing the impedance rise indicate a consistent increase throughout the soc range for SEI ageing, with the highest increase observed. In case of LAM ageing, a larger increase is noted only in the lower OCV region, and for plating, two regions with peaks in fundamental response increase are evident but with lesser magnitude compared to other two ageing modes. This underscores the importance of a comprehensive analysis that extends beyond a singular SOC level. The effects observed across different frequency ranges align with findings from prior work [10,11]. Notably, no quantifiable effect is shown above a frequency of 15 Hz. The observed effects of the three ageing mechanisms indicate a region of particular variation in the mid and lower OCV ranges, and therefore, we have chosen to concentrate our subsequent analysis in this region.

3.3. Regression model results

The extent of degradation for ageing modes considered for the study was quantified directly in the PyBaMM output in terms of two key parameters: loss of lithium inventory (LLI%) and Loss of active material in negative electrode (LossLAM). The total LLI% is contributed

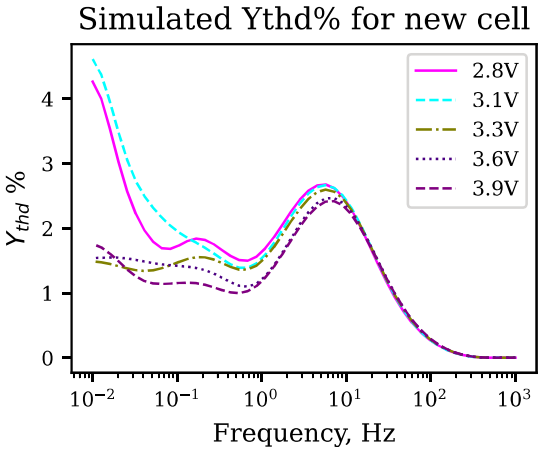

Fig. 5. Simulated NFRA spectra at multiple OCVs.

by loss from plating (lossPl) and due to SEI growth (lossSEI) and corresponding loss percentage are calculated from PyBaMM output capacity loss parameter as shown in Eqs. (4) and (5) below.

$$lossPl = \frac{\text{Capacity loss to plating} \times \text{LLI\%}}{\text{Total capacity loss to side reaction}} \tag{4}$$

$$lossSEI = \frac{\text{Capacity loss to SEI} \times \text{LLI\%}}{\text{total capacity loss to side reaction}} \tag{5}$$

As discussed in Section 2.4, in this study we tried to correlate the following predictors OCV, delta values of Y_F, Y_2%, Y_3%, Y_{thd}%, and ratio of Y_2%, and Y_3% in the characteristic frequency range to the ageing losses. First step to facilitate this correlation was normalizing each of these predictors, while an initial attempt involved employing a carpet parametrization, the disparate ranges of values for each parameter necessitated individual normalization. Subsequently, a feature ranking algorithm was applied to identify the most significant predictors influencing the ageing losses. For the regression analysis, the **MLPRegressor** from **sklearn.neural_network** module was employed. The standardization of predictor data was done using **StandardScaler** from **sklearn.preprocessing**. Feature importance was obtained using the python module **permutation_importance** from the library **sklearn.inspection**. The dataset were split into training and validation sets with a ratio of 70% and 30% respectively, ensuring a balanced representation to robustly validate the predictive performance of the regression model. As predictors, a comprehensive set of 200 parameters, each of the Y_s mentioned earlier from 50 different frequencies, along with the OCV values were used. Random Forest Regressor (RF) was selected for model generation, by virtue of being well suited for application to highly-dimensional datasets, offering resistance to over fitting and delivering reliable predictions [17]. The intentional inclusion of parameters at higher frequencies, even in the absence of visible changes,

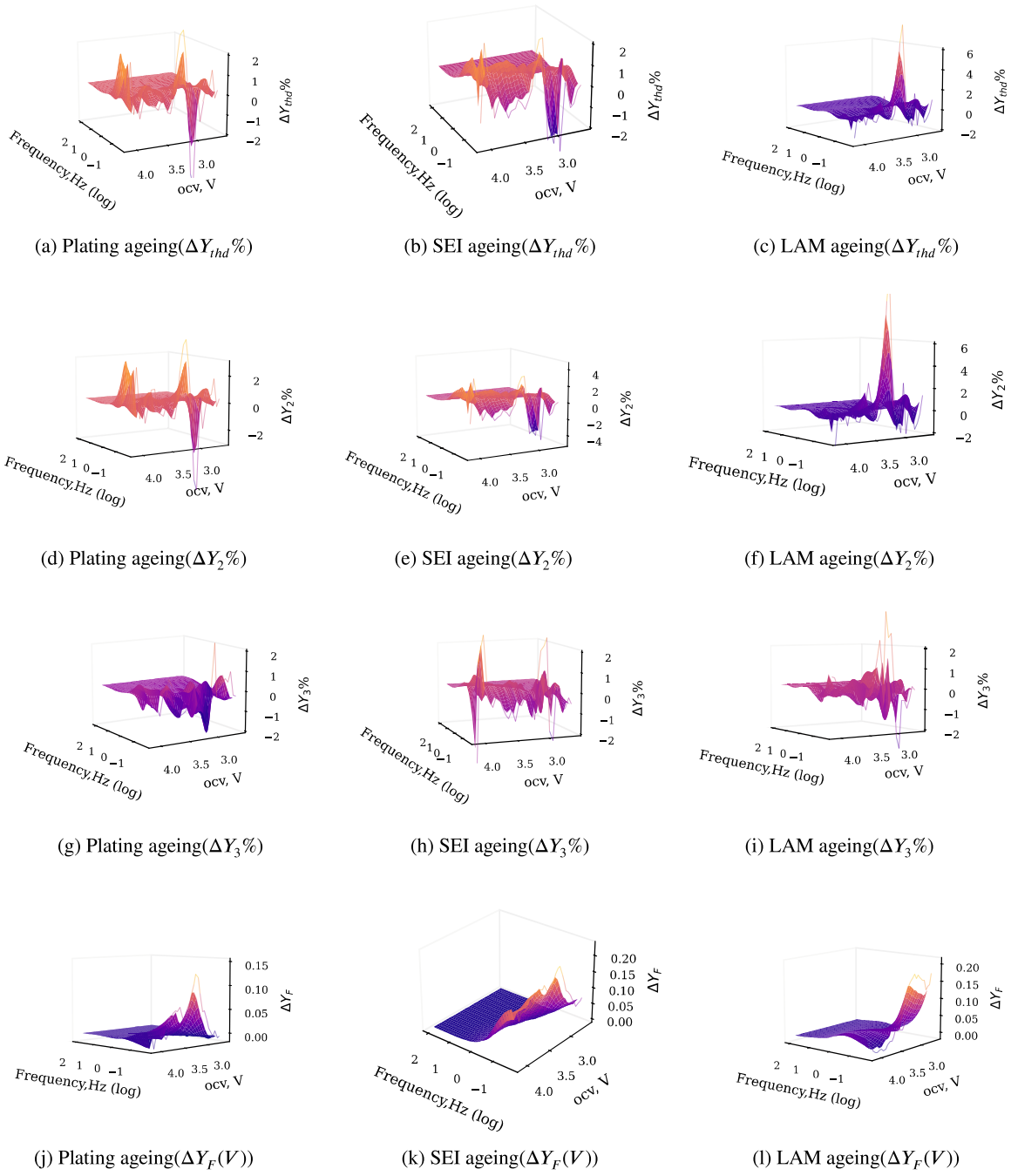

(a) Plating ageing($\Delta Y_{thd}\%$) (b) SEI ageing($\Delta Y_{thd}\%$) (c) LAM ageing($\Delta Y_{thd}\%$)

(d) Plating ageing($\Delta Y_2\%$) (e) SEI ageing($\Delta Y_2\%$) (f) LAM ageing($\Delta Y_2\%$)

(g) Plating ageing($\Delta Y_3\%$) (h) SEI ageing($\Delta Y_3\%$) (i) LAM ageing($\Delta Y_3\%$)

(j) Plating ageing($\Delta Y_F(V)$) (k) SEI ageing($\Delta Y_F(V)$) (l) LAM ageing($\Delta Y_F(V)$)

Fig. 6. 3D characteristic spectra for $\Delta Y_s\%$ response (a–c : $\Delta Y_{thd}\%$, d–f : $\Delta Y_2\%$, g–i : $\Delta Y_3\%$, j–l : $\Delta Y_F(V)$), versus frequency (log scale), and OCV for individual ageing.

aimed to uncover potential hidden information. Correlations between regression model output and PyBaMM simulated training/validation data are shown in Fig. 7 for each of the degradation modes with the top 5 ranked predictors. Good correlations were obtained for all ageing mechanisms with R^2 values around 0.98. The LAM model displayed the best correlation. The feature ranking provides insight into the sensitivity of predictors to the degradation modes. The salient predictors for the LAM degradation mode pertained mainly to changes in Y_F, which in turn can be ascribed to straightforward changes in (linear) impedance. The growth of SEI was found to correlate most significantly with $\Delta Y_2\%$ at a higher fundamental frequency range of 300 Hz; a phenomenon not observed in experimental results and warranting further validation. Meanwhile, plating exhibited correlations with $\Delta Y_3\%$ in the fundamental frequency range 0.5–0.8 Hz. In addition, when attempting to derive correlation outcomes using the harmonic predictors mentioned earlier at any singular frequency along with frequency and OCV values as additional predictors, it became evident that the formulated model yielded suboptimal results for predicting loss percentages. The R^2 values were notably lower, around 0.75. These findings underscore the necessity of integrating predictors across multiple frequencies along with OCV values to establish robust correlations.

3.4. Model application to experimental NFRA data

The trained RF models were applied to experimental NFRA data measured at an OCV of 3.3 V on cells subjected to distinct ageing protocols as described in Section 2.2. As discussed in Section 3.2, the regression model was trained on the NFRA data in the lower ocv range

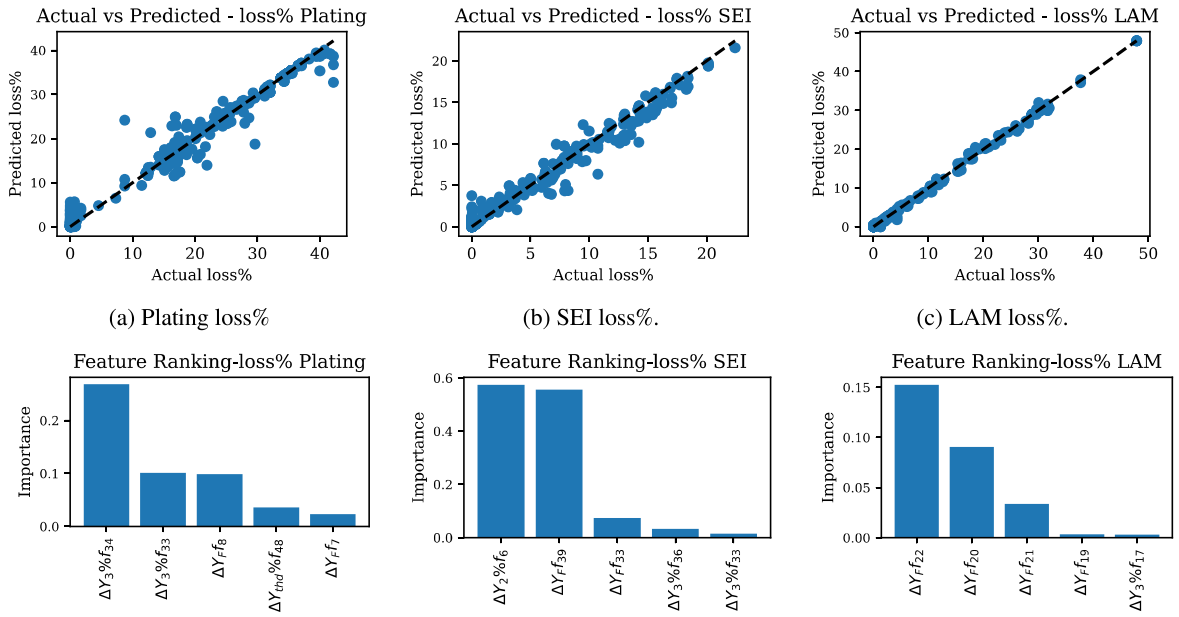

(a) Plating loss% (b) SEI loss%. (c) LAM loss%.

Fig. 7. Results for regression fit using harmonic predictors in the ocv range 2.8 to 3.6 V.

(2.8–3.6 V), wherein the most pronounced variations were observed. Furthermore, as the experimental data showed significant reduction of harmonic values (variations < 0.5%) for 3.6 V and 3.9 V, these data were not considered for model validation. The harmonic data obtained at 3.3 V were preprocessed with employing the same normalization technique before feeding into the RF models. The loss percentages, computed by the RF models from the NFRA data, for a group of cells with a comparable SOHs, (all within the 78%–83% range) are summarized in Fig. 8. The details of cyclic ageing of the selected cells are given in Table 4. This SOH range (78%–83%) was chosen because it contained a comparable number of cells tested at different temperatures. It is important to note that, due to the nature of accelerated ageing tests, obtaining a larger number of cells falling within similar SOH groups posed a considerable challenge. NFRA testing intervals were based on number of cycles and controlling for similar SOH degradation was inherently difficult. It is also crucial that cells of similar SOH need to be compared not based on cycle number, because subjecting cells to a same number of cycles under varied ageing conditions can result in different extents of degradation. The results obtained underscore the RF models' effectiveness in predicting and quantifying their respective ageing modes. In Fig. 8, the bars are colour-coded according to ageing temperature conditions: green bars correspond to cells cycled at lower temperatures (−5 °C and 10 °C), blue bars represent cycling at 25 °C, and red bars depict cycling at 45 °C and 50 °C. The RF models estimate more pronounced plating loss in cells aged at lower temperatures, as anticipated, and increased SEI growth loss in cells aged at higher temperatures, aligning with existing knowledge in the field [14]. It is noteworthy that the RF models estimate significant LAM and plating degradation across all the ageing conditions, which is perhaps due to the aggressive nature of ageing tests which employed relatively high rate charge and discharge vs the cell manufacturer's datasheet specification. While our approach provides a degree of qualitative verification, obtaining quantitative validation on experimental cells requires an extensive postmortem tear-down analysis to independently quantify the extent of each degradation modes, an exercise which remains for future work.

Table 4
Cell ageing details.

Cell No:	C-rate	Temperature Ageing (°C)	SOH (%)
C_1	0.5C	−5	81.7
C_2, C_3	1C	10	82.3, 78.7
C_4, C_5	1C	25	78.9, 78.7
C_6, C_7			81.1, 80.1
C_8	1C	45	81.5
C_9	0.5C	50	79.1

4. Conclusion

In this study, we have demonstrated the application of a regression modelling approach, trained on data simulated via a P2D cell model, for identifying the ageing history of lithium-ion batteries from nonlinear frequency response analysis (NFRA) measurements. By individually quantifying the extent of major degradation modes, such as SEI growth, lithium plating, and LAM, using the NFRA method, we have gained valuable insights into the ageing history of these batteries. Our analysis, conducted using both experimental and simulation approaches, has revealed the ability of P2D modelling to simulate NFRA responses and, in turn, for NFRA to act as a powerful diagnostic tool for elucidation of battery ageing mechanisms. Simulated NFRA spectra, which are in good qualitative agreement with experimental measurements, have shown a clear dependence on the ageing pathway, indicating that NFRA can effectively capture the ageing-induced changes in battery behaviour. However, it is important to highlight that the qualitative nature of the harmonic spectra remained similar during ageing, suggesting that the absolute values of NFRA measurements alone is inadequate for distinguishing between various ageing modes. The delta harmonic values, which represent the change in response vs. beginning of life are better predictors of the ageing mechanisms than the absolute values. Additionally, the change in NFRA responses are not always monotonous with ageing, and the variations are highly influenced by the state of charge (SOC) at which the measurements are taken. Our observations indicate that harmonic distortions (Y_{thd}%) in the fundamental frequency range 0.2–10 Hz exhibits a decreasing trend with ageing at lower open circuit voltages (OCVs) and an increasing trend at higher OCVs. The three ageing modes discussed here exhibited reasonable sensitivities in the mid and lower OCV range. The feature ranking analysis revealed that harmonic predictors with high-ranked values were mostly in the frequency range of 0.2 to 10 Hz. Interestingly, the SEI growth ageing mode showed a significant correlation with the change in Y_2 value at a

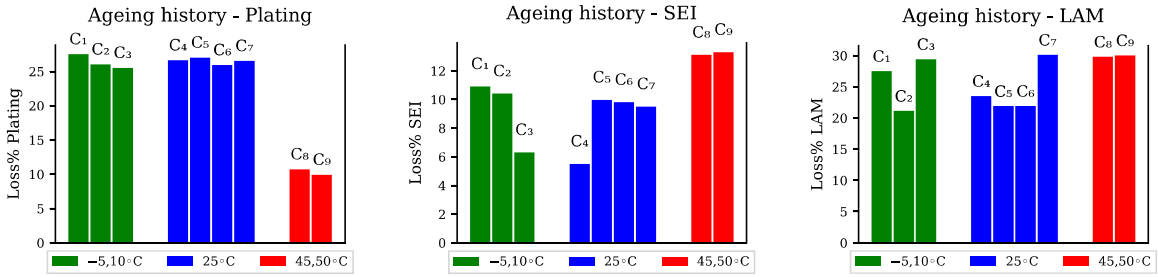

(a) Age history Plating%(3.3V) (b) Age history SEI%(3.3V) (c) Age history LAM%(3.3V)

Fig. 8. Model prediction on experimental data based on Table 4 ageing conditions at 3.3 V for soh group 78%–83%. (For interpretation of the references to colour in this figure legend, the reader is referred to the web version of this article.)

frequency near 300 Hz. The regression analysis results demonstrate that for a comprehensive understanding of different ageing modes, NFRA measurements are required at multiple OCVs and different fundamental frequencies. Single OCV, single frequency values are not sufficient for accurate ageing assessment. The application of these novel techniques to a practically-relevant cell format and chemistry in this study further highlights the potential for NFRA and the associated analytical and modelling approaches for industrial application, wherever there is a need for detailed assessment of battery SOH and estimation of remaining useful life. By providing a quantitative and data-driven approach to battery ageing assessment, NFRA has the potential to significantly improve battery management strategies to extend battery lifespan and also to evaluate suitability for second life applications. The areas open for future work are particularly in terms of improving the robustness of regression analysis, reducing dimensionality, and broadening testing conditions and also application to other lithium ion chemistries.

CRediT authorship contribution statement

Safeer Rahman O.C.: Writing – review & editing, Writing – original draft, Validation, Software, Methodology, Formal analysis, Data curation, Conceptualization. **Simon Shepherd:** Writing – review, Supervision, Methodology, Funding acquisition. **Quirin Kellner:** Writing – review, Supervision. **Oliver Curnick:** Writing – review & editing, Visualization, Supervision, Project administration, Methodology, Conceptualization.

Declaration of competing interest

The authors declare the following financial interests/personal relationships which may be considered as potential competing interests: Safeer Rahman Ottakath Cholakkal reports financial support was provided by FEV UK LTD. If there are other authors, they declare that they have no known competing financial interests or personal relationships that could have appeared to influence the work reported in this paper.

Data availability

Data will be made available on request.

References

[1] Christoph R. Birkl, Matthew R. Roberts, Euan McTurk, Peter G. Bruce, David A. Howey, Degradation diagnostics for lithium ion cells, J. Power Sources 341 (2017) 373–386.

[2] Jacqueline S. Edge, Simon O'Kane, Ryan Prosser, Niall D. Kirkaldy, Anisha N. Patel, Alastair Hales, Abir Ghosh, Weilong Ai, Jingyi Chen, Jiang Yang, Shen Li, Mei Chin Pang, Laura Bravo Diaz, Anna Tomaszewska, M. Waseem Marzook, Karthik N. Radhakrishnan, Huizhi Wang, Yatish Patel, Billy Wu, Gregory J. Offer, Lithium ion battery degradation: what you need to know, Phys. Chem. Chem. Phys. 23 (14) (2021) 8200–8221.

[3] Markus Schindler, Johannes Sturm, Sebastian Ludwig, Axel Durdel, Andreas Jossen, Comprehensive analysis of the aging behavior of nickel-rich, silicon-graphite lithium-ion cells subject to varying temperature and charging profiles, J. Electrochem. Soc. 168 (6) (2021) 060522.

[4] Thomas Waldmann, Marcel Wilka, Michael Kasper, Meike Fleischhammer, Margret Wohlfahrt-Mehrens, Temperature dependent ageing mechanisms in lithium-ion batteries - a post-mortem study, J. Power Sources 262 (2014) 129–135.

[5] Mohamed Elmahallawy, Tarek Elfouly, Ali Alouani, Ahmed Massoud, A comprehensive review of lithium-ion batteries modeling, and state of health and remaining useful lifetime prediction, IEEE Access 10 (September) (2022) 1–1.

[6] Erika Teliz, Carlos F. Zinola, Verónica Díaz, Identification and quantification of ageing mechanisms in Li-ion batteries by electrochemical impedance spectroscopy., Electrochim. Acta 426 (April) (2022).

[7] Björn Rumberg, Bernd Epding, Ina Stradtmann, Arno Kwade, Identification of Li ion battery cell aging mechanisms by half-cell and full-cell open-circuit-voltage characteristic analysis, J. Energy Storage 25 (March) (2019) 100890.

[8] Nicolas Wolff, Nina Harting, Marco Heinrich, Ulrike Krewer, Nonlinear frequency response analysis on lithium-ion batteries: Process identification and differences between transient and steady-state behavior, Electrochim. Acta 298 (2019) 788–798.

[9] Nina Harting, Nicolas Wolff, Fridolin Röder, Ulrike Krewer, State-of-health diagnosis of lithium-ion batteries using nonlinear frequency response analysis, J. Electrochem. Soc. 166 (2) (2019) A277–A285.

[10] Nina Harting, Nicolas Wolff, Fridolin Röder, Ulrike Krewer, Nonlinear frequency response analysis (NFRA) of lithium-ion batteries, Electrochim. Acta 248 (2017) 133–139.

[11] Nina Harting, Nicolas Wolff, Ulrike Krewer, Identification of lithium plating in lithium-ion batteries using nonlinear frequency response analysis (NFRA), Electrochim. Acta 281 (2018) 378–385.

[12] Danial Sarwar, Chongming Wang, Tazdin Amietszajew, Cheng Zhang, Chitta Saha, Oliver Curnick, Capacity fade detection in lithium-ion batteries using non-linear frequency response analysis (NFRA) under multiple open-circuit voltages (OCVs), Electrochem. Commun. 140 (June) (2022) 107338.

[13] Valentin Sulzer, Scott G. Marquis, Robert Timms, Martin Robinson, S. Jon Chapman, Python battery mathematical modelling (PyBaMM), J. Open Res. Softw. 9 (2021) 1–8.

[14] Simon E.J. O'Kane, Ian D. Campbell, Mohamed W.J. Marzook, Gregory J. Offer, Monica Marinescu, Physical origin of the differential voltage minimum associated with lithium plating in Li-ion batteries, J. Electrochem. Soc. 167 (9) (2020) 090540.

[15] Chang-Hui Chen, Ferran Brosa Planella, Kieran O'Regan, Dominika Gastol, W. Dhammika Widanage, Emma Kendrick, Development of experimental techniques for parameterization of multi-scale lithium-ion battery models, J. Electrochem. Soc. 167 (8) (2020) 080534.

[16] Buddhi Wimarshana, Izzuan Bin-Mat-Arishad, Ashley Fly, Parameter sensitivity analysis of a physico-chemical lithium-ion battery model with combined discharge voltage and electrochemical impedance data, J. Power Sources 527 (November 2021) (2022) 231125.

[17] Ziwei Jin, Jiaxing Shang, Qianwen Zhu, Chen Ling, Wu Xie, Baohua Qiang, RFRSF: Employee turnover prediction based on random forests and survival analysis, in: Lecture Notes in Computer Science (Including Subseries Lecture Notes in Artificial Intelligence and Lecture Notes in Bioinformatics), in: LNCS, vol. 12343, 2020, pp. 503–515.